Modal decomposition of hopping states in cellular flames

Antonio Palacios
Department of Mathematics, San Diego State University, San Diego, California 92812

Michael Gorman[a)]
Department of Physics, University of Houston, Houston, Texas 77204

Gemunu H. Gunaratne
Department of Physics, University of Houston, Houston, Texas 77204 and The Institute of Fundamental Studies, Kandy, Sri Lanka

(Received 30 December 1998; accepted for publication 1 April 1999)

We use Karhunen–Loeve (KL) decomposition of video images from an experiment to analyze a spatiotemporal dynamic state, unique to cellular flames, referred to as a ''hopping state.'' Ordered states of cellular flames on a circular burner consist of one or two concentric rings of luminous cells. The hopping states correspond to the motions of individual cells in a ring sequentially executing abrupt changes in their angular position, while the other cells in the ring remain symmetric and at rest. KL decomposition separates the spatial and temporal characteristics of the hopping motion. The underlying symmetries of the experiment allow us to deduce a set of normal form equations that describe the formation of these states. We find that they result from secondary bifurcations connecting two primary branches of traveling waves. The solutions corresponding to hopping states exist as mixed-mode solutions away from the secondary bifurcations. © *1999 American Institute of Physics.* [S1054-1500(99)02503-3]

In rotating wave (TW) states observed in cellular flames all N cells sweep out equal angles in equal times. In modulated rotating wave (MTW) states all N cells speed up and slowdown in unison. In hopping states individual cells (sequentially) abruptly change their angular positions, while the other $(N-1)$ cells are at rest (much like people moving up when a vacancy occurs in a line). In this paper we show that hopping states result from an interaction between an N cell TW state and an $(N-1)$ cell TW state, with different angular velocities; yet, the resulting hopping state is not a TW state.

I. INTRODUCTION

A flat, premixed flame is a propagating front of uniform chemical reaction. Heavy hydrocarbon–air mixtures form cellular flames in which regions of bright cells and darker cusps and folds reflect enhanced and diminished combustion due to the diffusion of the lighter oxygen relative to the heavier fuel. When the flame front is confined to a circular domain, the cells organize themselves in either stationary states of concentric rings or nonstationary states in which the cells can move collectively within the ring structure.

We have previously analyzed the dynamics of rotating states (TW), standing wave states (SW), and modulated rotating states (MTW) using Karhunen–Loeve (KL) decomposition with the aim of developing the appropriate normal forms.[1] The KL decomposition of a rotating ring of k cells showed the presence of $k-2k$ coupling. The normal form theory corresponding to these ''parity-broken'' states predicted the presence of modulated rotating states and standing wave states, which were also observed in the experiment in nearby regions of parameter space. The normal forms are obtained from the symmetries of the physical system and the symmetries of the modes, thus circumventing the need to use a detailed model of the flame front, for which calculations are extremely cumbersome.

In this paper we present a corresponding analysis of spatiotemporal states with unusual characteristics and considerably more complex dynamics. These states were earlier classified as ''square dance modes''[2] and later as ''hopping states.''[3] In numerical simulations from a thermodiffusive model, a similar state was termed ''Pushmi–Pullyu.''[4] The hopping states are formed by cells that sequentially make rapid changes of angular position while moving in a ring structure. The ring can be isolated or can be surrounded by a stationary ring.

The motion of cells in a hopping state is very different from that of a traveling wave state (TW) or a modulated traveling wave state (MTW).[5] In a TW state identical asymmetric cells of fixed shape rotate uniformly. In a MTW state identical asymmetric cells change their shapes periodically, while moving within the ring structure. In contrast, individual cells of a hopping state execute the same motions at different times. A single cell, whose shape is momentarily asymmetric, makes a rapid excursion to a new location, while the remaining cells stay in place. Each cell in the ring moves sequentially as described. To our knowledge, this kind of motion has not been observed in any other physical systems. Understanding the spatiotemporal dynamics of hopping states and contrasting them with the spatiotemporal dynamics of TWs and MTWs is the purpose of this work.

A description of the experimental apparatus and proper-

[a)]Electronic mail: gorman@uh.edu

ties of hopping states are given in Sec. II. With the aid of a phenomenological model (see Sec. III), we explore the stability of cellular flame patterns. The model helped us to identify the spatial structure of many stationary states in terms of Fourier–Bessel modes.[1] The essential features of Karhunen–Loève decomposition are described in Sec. IV. In Sec. V, we study various configurations with three hopping cells, which include a single ring of hopping cells and two concentric rings where a stationary ring surrounds a ring of hopping cells. The similarity in the behavior of the hopping cells in these two cases leads us to conclude that the interaction between rings is relatively weak. We thus concentrate on the analysis of single ring patterns and demonstrate that hopping states with three cells result from the Hopf–Hopf interaction of a two-cell TW with a three-cell TW. These states exist as mixed-mode solutions away from the secondary bifurcations. We propose a normal form for the system and show how its output can be used to reconstruct the motion of cells in physical space. In Sec. VI, we generalize these results to other hopping states.

II. CLASSIFICATION OF EXPERIMENTAL STATES

The experimental flame patterns are stabilized on a circular porous plug that burns premixed gases inside a low pressure (0.3–0.5 atm) combustion chamber. Pressure, flow rate, and fuel/oxidizer ratio are the principal parameters that determine the formation of the patterns. In these experiments a steady uniform flame in the form of a circular luminous disk, 5.62 cm in diameter and 0.5 mm thick, sits 5 mm above the surface of the burner. We call this initial state the ''uniform state'' of the experiment and note that it inherits the circular symmetry of the burner. To the experimentalist, the uniform state looks the same if the burner is rotated by an arbitrary angle, or if the experiment is observed through a vertical mirror. It is then reasonable to identify $O(2)$, the group of rotations and reflections on the plane, as the underlying group of symmetries of these flame experiments.

Upon changes of control parameters, the $O(2)$ symmetric uniform solution loses stability, and the flame front forms ordered patterns of concentric rings of cells. Brighter cells correspond to hotter regions closer to the burner. They are separated by darker regions corresponding to cusps and folds which extend an additional 5 mm away from the surface of the burner. The cellular patterns include stationary states and dynamical states in which the cells are able to move within the ring configuration. The stationary states can be classified based on their spatial symmetries. Usually, a subgroup of $O(2)$ suffices for stationary states consisting of a single ring of cells while those states with two rings can be described by direct products of subgroups. In contrast, both spatial and temporal symmetries must be taken into account when describing dynamical states.

Hopping states appear in patterns with either one or two rings of cells at parameter values for which two ordered states compete for stability. For instance, a hopping state with three cells is found in a range of parameter values between those where three-cell ordered states and four-cell ordered states are stable. Hopping states have been observed in butane–air and isobutane–air flames, but not in propane–air flames. Figure 1 depicts four different configurations of hopping states. In Figs. 1(a) and 1(d), hopping occurs in a single ring array of cells, while in Figs. 1(b) and 1(c), an inner ring of hopping cells is surrounded by a stationary outer ring.

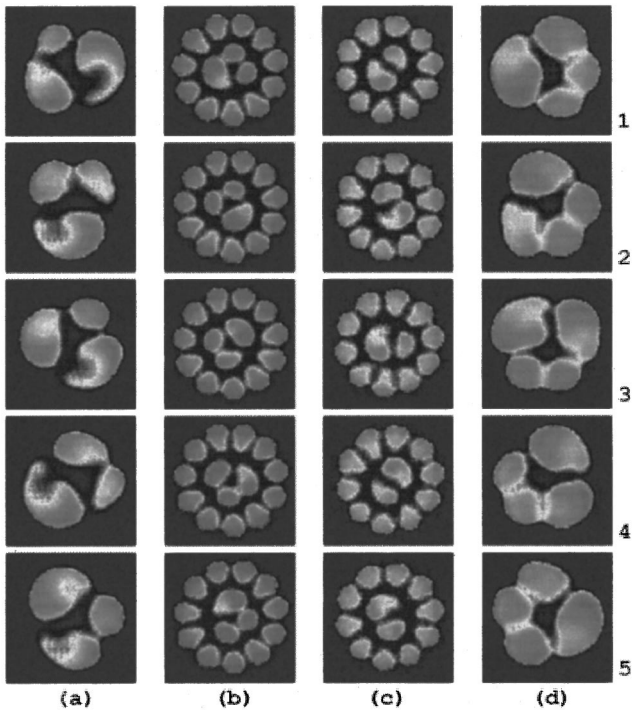

FIG. 1. Four sequential frames of videotape of four different experimental states with hopping motion in: (a) a single ring state with three cells; (b) an inner ring of three cells surrounded by a stationary outer ring with eleven cells; (c) an inner ring of two cells surrounded by a stationary outer ring with ten cells; (d) a single ring state with four cells.

In order to study the spatiotemporal characteristics of the motion, the evolution of the flame front is recorded with a Dage-MTI charge-coupled device (CCD) camera, mounted vertically on top of the combustion chamber. The video images capture the emitted chemiluminescence from the flame front and provide a two-dimensional measurement proportional to the temperature at various points on the burner. Such measurements are commonly used in flame models.[6–8] The spatial and temporal resolution, the time interval, and the dynamic range are limited only by the recording device. Images of 640×480 pixel resolution, taken at 1/30 s intervals with 7 bit dynamic range, are typical for dynamics recorded on S-VHS video tape.

III. MATHEMATICAL MODEL

In previous work,[1] we investigated the formation and evolution of cellular patterns in circular domains with a reaction–diffusion PDE system in the form

$$\begin{aligned}\partial_t u &= (B-1)u + A^2 v - \eta u^3 - \nu_1(\nabla u)^2 + \kappa_1 \nabla^2 u,\\ \partial_t v &= -Bu - A^2 v - \eta v^3 - \nu_2(\nabla v)^2 + \kappa_2 \nabla^2 v,\end{aligned} \tag{1}$$

where $u(\mathbf{x},t)$ and $v(\mathbf{x},t)$ are two linearly coupled, diffusive spatiotemporal fields with diffusion coefficients κ_1 and κ_2, respectively. The cubic terms control the growth of the lin-

early unstable modes, while the nonlinear gradient terms render the model nonvariational. Several stationary and nonstationary patterns whose characteristics are similar to the experimental states were observed in the model.

These corresponding states from the model complement the experimental results by giving insight into the dynamics of hopping motion. Due to the circular geometry of the domain, the integration of Eq. (1) is carried out in polar coordinates $\mathbf{x}=(r,\theta)$ over a circular grid of radius R. An alternating direction implicit algorithm is used in the numerical integration procedure.[9] Since qualitatively different patterns are observed as R is varied, the radius of the burner will be treated as a distinguished bifurcation parameter.

A. Linear stability analysis

A scalar field $u(r,\theta,t)$ satisfying Dirichlet boundary conditions on a circular domain of radius R can be expanded as

$$u(r,\theta,t)=\sum_{n,m} z_{nm}(t)\Psi_{nm}(r,\theta)+\text{c.c.}, \tag{2}$$

where $\Psi_{nm}(r,\theta)=J_n(\alpha_{nm}r/R)e^{in\theta}$, $(m\geqslant 0$ and $n>0)$ and c.c. denotes complex conjugate.[10] Here $J_n(r)$ is the nth-order Bessel function of the first kind and α_{nm} is its mth-nontrivial zero. z_{nm} are complex time-dependent coefficients, save for z_{0m} which are real. The orthonormality and completeness of the functions $\{\Psi_{nm}(r,\theta):n\geqslant 0,m\geqslant 1\}$ gives

$$z_{nm}(t)=\frac{1}{\pi R^2 J_{n+1}^2(\alpha_{nm})}\times\int_0^{2\pi}\int_0^R ru(r,\theta,t)\overline{\Psi}_{nm}(r,\theta)\,d\theta\,dr, \tag{3}$$

with the proviso that the coefficients are half of the value given when $n=0$.

Previously, the linear stability of the uniform state $(u_0,v_0)=(0,0)$ was studied by considering small perturbations $\mathbf{w}=(w_u,w_v)$ proportional to Fourier–Bessel functions

$$\mathbf{w}=e^{\lambda t}\Psi_{nm}(r,\theta). \tag{4}$$

Under these perturbations, the uniform state (u_0,v_0) is stable if $\lambda<0$, and unstable if $\lambda>0$. The marginal stability curve corresponds to those parameters where $\lambda=0$ and was calculated as a function of the distinguished parameter R,

$$B_{nm}^M(R)=1+\frac{\kappa_1}{\kappa_2}A^2+\kappa_1\left(\frac{\alpha_{nm}}{R}\right)^2+\frac{A^2}{\kappa_2}\left(\frac{R}{\alpha_{nm}}\right)^2. \tag{5}$$

Beyond this curve, on increasing B, the uniform state destabilizes to $\Psi_{nm}(r,\theta)$. For a given value of A, a particular curve B_{nm} reaches a minimum value of

$$B_0=1+\frac{\kappa_1}{\kappa_2}A^2+2A\sqrt{\frac{\kappa_1}{\kappa_2}} \tag{6}$$

at a radius $R=\alpha_{nm}(\kappa_1\kappa_2/A^2)^{1/4}$. The results presented in this paper are evaluated with fixed values of $\kappa_1=1.6$, $\kappa_2=16.0$, $\eta=0.8$, $\nu_1=2.32$, $\nu_2=6.501$, and $A=5.0$. B and R are used as control parameters.

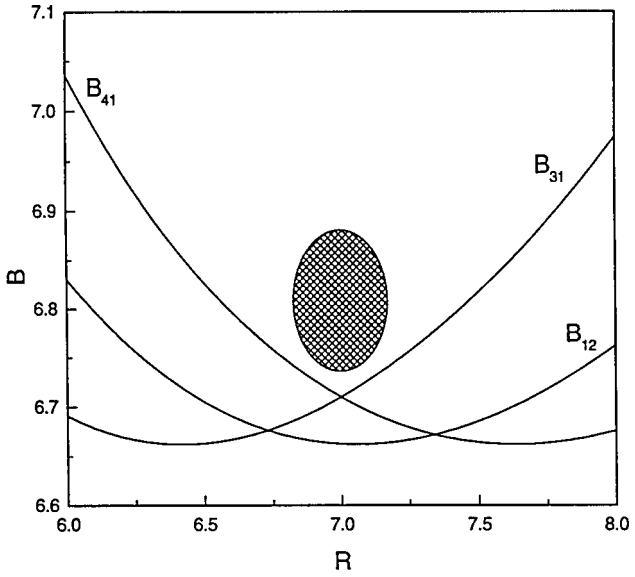

FIG. 2. Marginal stability curves defining the stability domains where the trivial solution $(u_0,v_0)=(0,0)$, representing a uniform flame front, bifurcates to Fourier–Bessel modes Ψ_{nm}.

B. Numerical results

The integration of Eq. (1) was focused in a region where the evolution of a single ring pattern with three cells can be traced. Such region can be found in a neighborhood of the minimum of the marginal stability curve B_{31} shown in Fig. 2. As the curved is crossed, on increasing B, a stationary pattern of three cells with purely spatial D_3 symmetry bifurcates from the $O(2)$ symmetric trivial solution. Increasing B further, the shaded region is found, in which the three-cell pattern is no longer dominant but rather competes for stability with another stationary ring of four cells. To the left of the region, the three-cell state is stable; and to the right, the four-cell state becomes the dominant mode.

Consider now the stationary ring of three cells as observed to the left of the shaded region. On moving right, the D_3 symmetry of the ring is broken and a nonstationary pattern bifurcates subcritically. Figure 3 depicts various snapshots of the evolution of $u(r,\theta,t)$. The bifurcating field also contains three cells but now the cells rotate clockwise. The

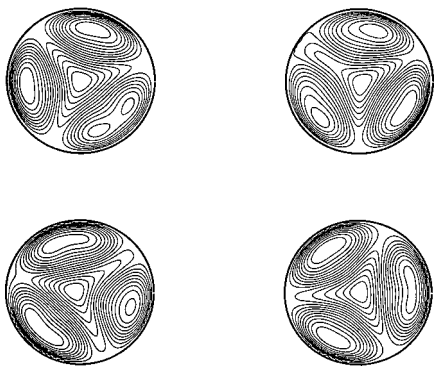

FIG. 3. Space and time evolution of three cells hopping from model (1). The cells move nonuniformly and their shapes change periodically. Observe the competition with a four-cells state.

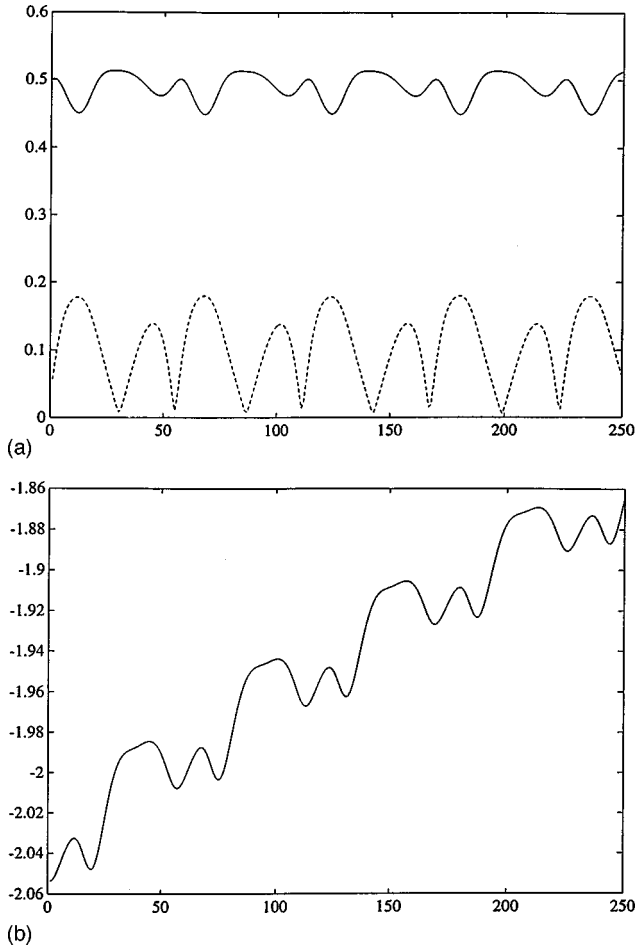

FIG. 4. Time evolution of the (a) amplitude coefficients and their (b) corresponding phases, found in the Fourier–Bessel decomposition of the hopping state shown in Fig. 3. The observed modulations indicate the presence of nonuniform motion.

ring of cells rotates nonuniformly with the shape of each cell changing periodically. The dynamics of each cell is more complicated. An animated sequence of the field reveals small but visible jumps in the angular position of each cell. One of the cells changes its shape more than the other two and also appears more asymmetric. In comparison with experimental observations of hopping states, the jumps in angular positions are smaller in magnitude but, up to a time scale factor, the general characteristics of the dynamics are very similar. Figure 4 shows the time evolution of the amplitude and phases of a few coefficients in the Fourier–Bessel decomposition of $u(\mathbf{x},t)$. The amplitude modulations reflect the shape changes of the cells, and the phase modulations confirm the nonuniform rotation of the cells. The periodicity of the modulations further suggests that this nonstationary pattern is created via a Hopf bifurcation. The frequency spectrum (not shown) of the Fourier–Bessel coefficients indicates the presence of two incommensurate frequencies and their harmonics. This quasiperiodic motion of the cells can be easily visualized in the phase plane projections of the space $(z_{11},z_{21},z_{31},z_{41})$, which is shown in Fig. 5. A computer animation of the numerical results is posted in the World Wide Web at http://vip.cs.utsa.edu/flames/klvisual/klvisual.html.

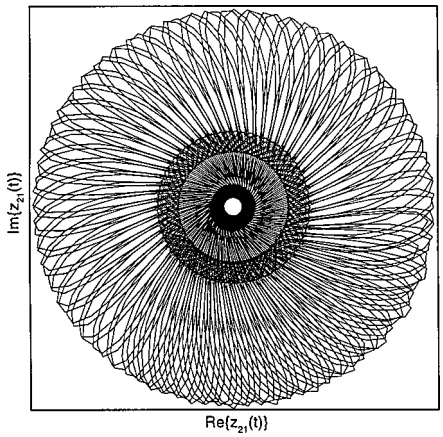

FIG. 5. Phase plane projections of real and imaginary parts of the most dominant Fourier–Bessel coefficients obtained in the decomposition of the hopping state shown in Fig. 3. The modulations in the angular motion of the cells is clearly visible in the projections.

IV. KARHUNEN–LOÈVE DECOMPOSITION OF EXPERIMENTAL DATA

Let $u(\mathbf{x},t):D\rightarrow R$ be a scalar-valued function representing an observable of a numerical or physical experiment, where $D\subset R^n$ is the domain of the experiment and t represents time. Karhunen–Loève decomposition[11–15] allows us to separate the spatial and temporal variations of $u(\mathbf{x},t)$ by extracting time-independent orthonormal basis functions $\Phi_k(\mathbf{x})$, and time-dependent orthonormal amplitude coefficients $a_k(t)$, such that the reconstruction

$$u(\mathbf{x},t)=\sum_k a_k(t)\Phi_k(\mathbf{x}) \tag{7}$$

is optimal in the sense that the average least-squares truncation error in the approximation up to Nth order

$$\epsilon_N=\left\langle \left\| u(\mathbf{x},t)-\sum_{k=1}^{N} a_k(t)\Phi_k(\mathbf{x}) \right\|^2 \right\rangle \tag{8}$$

is always a minimum for any given number N of basis functions over all possible sets of orthogonal functions.

The observable can be a continuous function of space and time or a discrete set of vector-valued functions. For instance, in Rayleigh–Benard convection,[16] in which a fluid confined between two parallel plates is heated from below, $u(\mathbf{x},t)$ can be assumed to be a component of a velocity field, and $D=\{(x,y,z):0<z<1\}$ a region between the two plates. In Eq. (1), $u(\mathbf{x},t)$ could be any of the two diffusive spatiotemporal fields that simulate the evolution of cellular flames. In the combustion experiments of Sec. II, u is a function of the intensity of the light emitted by the flame front, and D is the circular burner. Since the variations in light intensity are recorded on video tape, u is now a discrete vector of video images. Each image is a $N=w\times h$ array of pixels with scalar values in the range $[0, 255]$. Formally, u is represented by a discrete sequence of M data vectors of the form $\mathbf{u}_i(\mathbf{x})=[u(x_1,t_i),u(x_2,t_i),\ldots,u(x_N,t_i)]^T$, $i=1...M$, where x_j is the jth grid point in the pixel domain D

$=(x_1,x_2,...,x_N)$, t_i is a discrete-time variable or frame index, and M indicates the total number of measurements of the experiment.

The functions $\Phi_k(\mathbf{x})$, called *empirical eigenfunctions, coherent structures*, or *KL modes*, are the eigenvectors of the *two-point spatial correlation* function which in the case of a discrete observable is given by

$$r(\mathbf{x},\mathbf{y})=\frac{1}{M}\sum_{i=1}^{M} u(\mathbf{x},t_i)u^T(\mathbf{y},t_i), \tag{9}$$

where $a_0(t)$ is a constant and Φ_0 is the time average of the data $\tilde{u}=(1/M)\Sigma_{i=1}^{M} u(\mathbf{x},t_i)$. Frequently, we are more interested in the variations of a data set u about its average value than on u itself. It is then common practice to subtract the average value from the data set prior to the KL decomposition and assume $\Phi_0=0$. However, when the original data set is reconstructed with Eq. (7), the average $\tilde{u}$ must be restored.

The method of snapshots. A direct computation of the eigenvectors of Eq. (9) involves solving the eigenvalue problem

$$r(\mathbf{x},\mathbf{y})\Phi(\mathbf{y})=\lambda\Phi(\mathbf{x}). \tag{10}$$

Since $r(\mathbf{x},\mathbf{y})$ is an $N\times N$ matrix, solving Eq. (10) could be a very expensive process if the number of grid points N is very large. However, when N is larger than the number of measurements M, then the *method of snapshots*[15] provides a popular and efficient alternative for solving the eigenvalue problem (10). The method is based on the fact that the data vectors $\mathbf{u}_i$, and the eigenvectors Φ_k, span the same linear space.[11,15] This result implies that the eigenvectors can be written as a linear combination of the data vectors

$$\Phi_k=\sum_{i=1}^{M} v_i^k\mathbf{u}_i. \tag{11}$$

After substitution in the eigenvalue problem (10), the coefficients v_i^k are obtained from the solution of

$$C\mathbf{v}=\lambda\mathbf{v}, \tag{12}$$

where $\mathbf{v}^k=(v_1^k,\ldots,v_N^k)$ is the kth eigenvector of Eq. (12), and C is a symmetric $M\times M$ matrix defined by $[c_{ij}]=(1/M)(\mathbf{u}_i,\mathbf{u}_j)$, where $(\cdot,\cdot)$ denotes the standard vector inner product, $(\mathbf{u}_i,\mathbf{u}_j)=u(x_1,t_i)u(x_1,t_j)+\cdots+u(x_N,t_i)u(x_N,t_j)$. In this way an $N\times N$ eigenvalue problem [the eigenvectors of Eq. (9)] is reduced to computing the eigenvectors of an $M\times M$ matrix, a preferable task if $N\gg M$. After computing the KL basis functions, the temporal coefficients $a_k(t)$ are calculated by projecting the data set onto each of the eigenfunctions

$$a_k(t)=\frac{(u(\mathbf{x},t),\Phi_k(\mathbf{x}))}{(\Phi_k(\mathbf{x}),\Phi_k(\mathbf{x}))}. \tag{13}$$

It can be shown that both temporal coefficients and eigenfunctions are uncorrelated in time and space (see the Appendix for more details). The results presented in this paper were obtained with an implementation of the method of snapshots through the use of the software package KLTOOL.[17]

V. HOPPING MOTION IN THREE CELLS

In this section, three different configurations of cellular patterns containing a ring of three hopping cells are analyzed. The first is a state with three hopping cells. The other two contain an inner ring of three hopping cells surrounded by a stationary outer ring. The dynamics of each state is encapsulated in a data set of the form $\mathbf{u}_i=[u(x_1,t_i),\ldots,u(x_N,t_i)]^T$, $i=1,...,M$, with $M=600$, frames and $N=4096$ pixels. Each data set is a digitization of 20 s of video tape at a rate of 30 frames/s.

The analysis presented in this section will reveal that these states result from the interaction of two traveling waves with incommensurate frequencies. The wave numbers are determined by the spatial symmetries of the modes, and they correspond, in physical space, to the number of cells in a ring. A reconstruction of the motion shows that the interaction of the two TWs produces a state with physical characteristics similar to those of the hopping states. The presence of the outer stationary ring of cells has no appreciable effect on the hopping motion of the inner ring of cells, suggesting that the interaction between the rings is very weak.

A. Hopping in a single ring pattern

The hopping motion in a single ring state with three cells is shown in Fig. 6(a). The label $3H$ has been assigned to this state in previous experimental studies.[3] The same classification scheme is adopted here. Five instantaneous snapshots of the data set, with time running from top-to-bottom, depict a cellular pattern with three cells rotating counterclockwise. Cells are numbered for identification purposes and frames are 1/15th s apart from each other. In frame 1, cell 1 is just finishing a hop. The cell behind it, cell 3, then begins to move in frame 2 and completes its hop in frame 3. It is then the turn for cell 2 to hop and its motion is completed in frame 4. In frame 5, the cycle repeats over again starting with cell 1. The hopping cell appears more asymmetric and moves faster than the other two cells, one of which is always at rest.

The application of KL decomposition gives the eigenfunctions shown in Fig. 6(b). The time average of the images $\tilde{u}$ (top snapshot), reflects the $O(2)$ symmetry of the burner, even though none of the instantaneous states has this symmetry.[18] Below the time average (ordered from left to right and top to bottom), the six most energetic KL modes $\Phi_1-\Phi_6$ are also depicted. The energy spectra (see the Appendix) $E=(15.1, 14.8, 12.1, 11.5, 5.4, 5.3, 4.6, 4.5, 1.9, 1.8,...)$ show an equal distribution of energy among consecutive pairs of modes, indicating that each pair of modes forms an invariant subspace for the overall dynamics. The reconstruction with the six most energetic modes is shown in Fig. 6(c). Since the KL modes were obtained directly from video images of the experiment, their analytical forms are unknown. However, their symmetries can be deduced through Fourier–Bessel decomposition. For the first three pairs, the largest contributions come from Fourier–Bessel modes Ψ_{21}, Ψ_{31}, and Ψ_{41}, respectively. This result confirms the visual perception of approximately D_2, D_3, and D_4 symmetry in each pair, respectively.

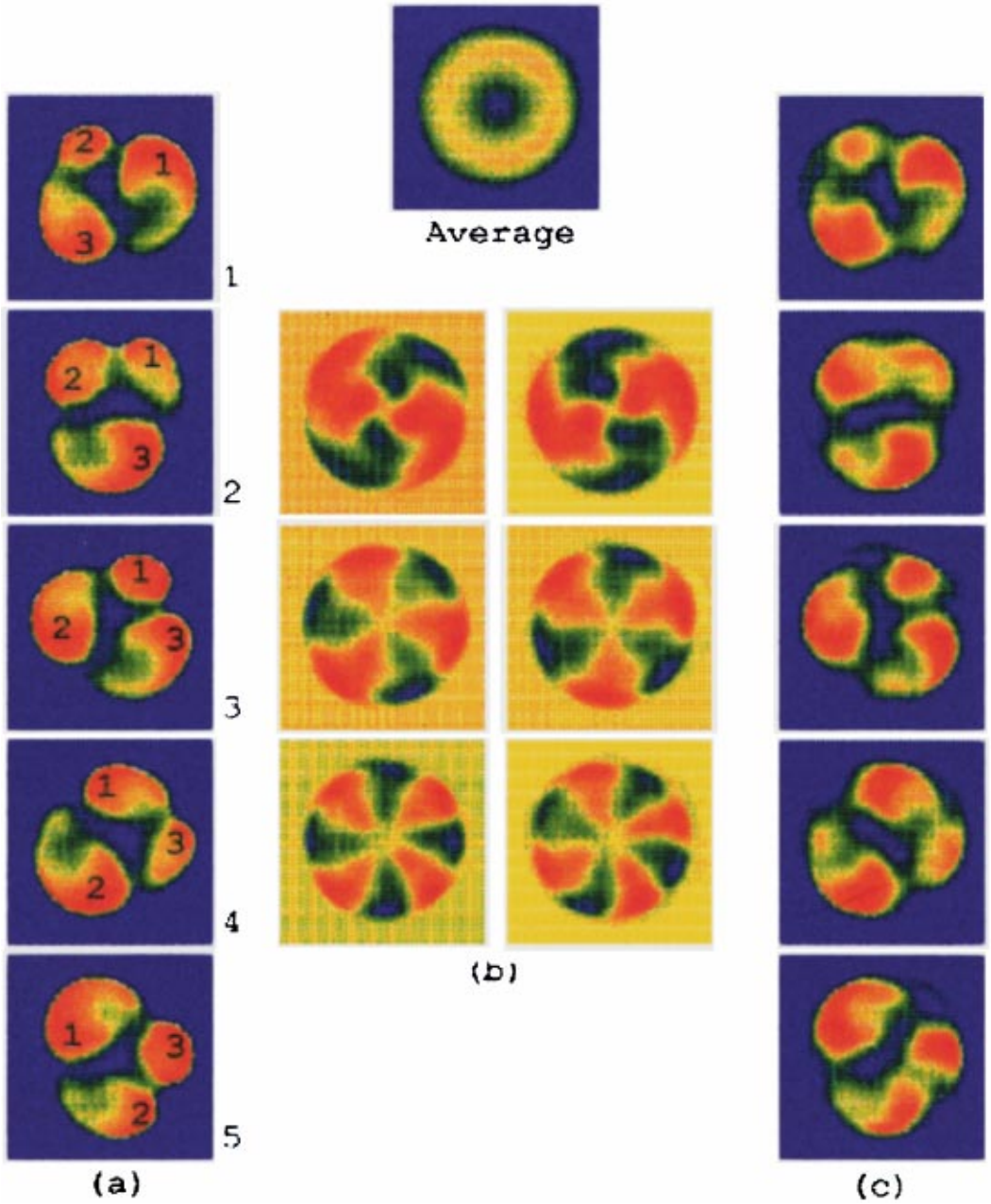

FIG. 6. KL decomposition of hopping motion in a single ring state with three cells: (a) five instantaneous snapshots showing hopping motion as the cells rotate counterclockwise; (b) the time average of the data set appears at the top, followed (from left-to-right and top-to-bottom) by the six most energetic modes $\Phi_1-\Phi_6$; (c) the reconstruction of the dynamics using the six most energetic KL modes.

Insight into the origin of the hopping motion can be obtained from the projections [see Eq. (13)] of the data set $\mathbf{u}_i(\mathbf{x})$ onto each invariant subspace. Using the two most energetic pairs of modes $\{\Phi_1,\Phi_2\}$ and $\{\Phi_3,\Phi_4\}$, the projections produce time coefficients $\{a_1(t),a_2(t)\}$ and $\{a_3(t),a_4(t)\}$, (not shown). The sinusoidal shape of the coefficients suggests that, on the invariant subspace $\{\Phi_1,\Phi_2\}$, the reconstructed dynamics

$$u(\mathbf{x},t)=\tilde{u}+a_1(t)\Phi_1(\mathbf{x})+a_2(t)\Phi_2(\mathbf{x}), \tag{14}$$

forms a cellular pattern of two traveling cells (TW_2^{3H}). Similarly, the reconstruction on the subspace $\{\Phi_3,\Phi_4\}$ forms a pattern of three traveling cells (TW_3^{3H}). The number of cells or wave number, is inferred from the spatial symmetries of the modes in each invariant space: D_2 and D_3, respectively. The phase difference observed in each pair is a consequence of the orthogonality (see the Appendix) of the modes, and it is needed to break the reflectional symmetry of the cells as required by the bifurcation of rotating waves from systems with $O(2)$ symmetry.[19]

Figure 7 shows the phase between the time coefficients associated with each wave, $\arctan(a_2(t)/a_1(t))$, and $\arctan(a_4(t)/a_3(t))$. The observed linear variation of the phases with slopes $m_2=1.1925$ and $m_3=0.8701$ indicates that each wave rotates uniformly. In physical space, the values of m_2 and m_3 correspond to angular speeds $w_2=17.67$ rad/s and $w_3=8.59$ rad/s, respectively. Observe that

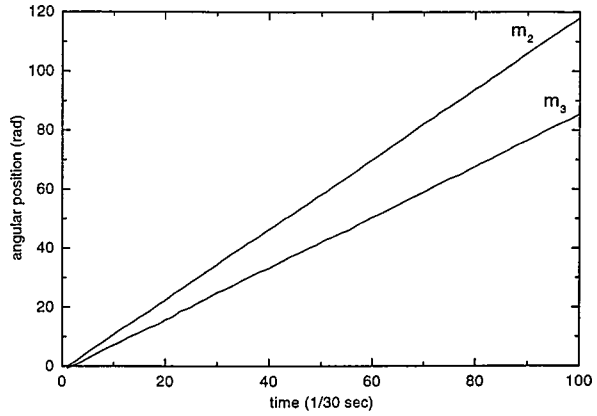

FIG. 7. The linear variation in the phase between $\{a_1(t),a_2(t)\}$ and $\{a_3(t),a_4(t)\}$ indicates uniform motion by the traveling waves TW_2^{3H} and TW_3^{3H}. The slopes of the phases, m_2 and m_3, are used to estimate the angular velocity of each wave, $\omega_2=17.67$ rad/s and $\omega_3=8.59$ rad/s, respectively.

TW_2^{3H} rotates significantly faster than TW_3^{3H}. The two-frequency motion can be visualized in the phase-plane projections of the space (a_1,a_2,a_3,a_4), as is shown in Fig. 8.

All these observations have been confirmed by viewing reconstructions in physical space with Eq. (7). The analysis is valid even though many modes have been omitted because, first, most of the remaining low energy modes capture only high-dimensional effects such as shape variations and, second, modes such as $\{\Phi_5,\Phi_6\}$ are higher harmonics of other modes, $\{\Phi_1,\Phi_2\}$ in this case. Up to a shape approximation, only four modes are needed to reproduce the dynamics.

B. Hopping motion in patterns with concentric rings

Figure 9(a) shows five sequential snapshots of a pattern with two concentric rings of cells. The outer ring contains eleven stationary cells, while the inner ring is formed by three cells hopping clockwise. This pattern is characterized as an $11/3H$ state. Cells in the inner ring hop in a fashion similar to those of the $3H$ state (but in the opposite sense). The stationary ring of outer cells has little effect on the motion of the inner cells.

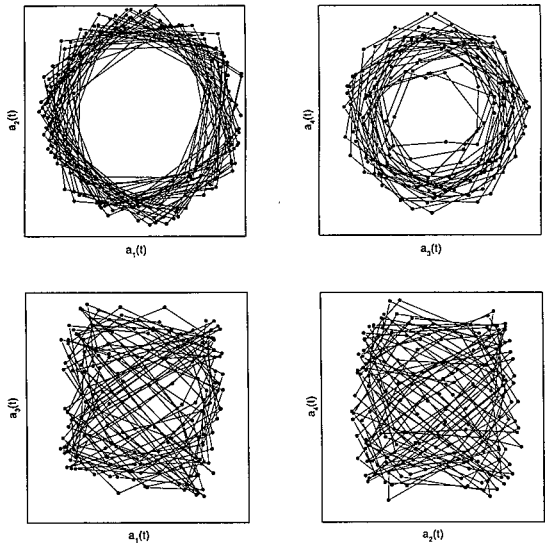

FIG. 8. Projections of phase plane $(a_1(t),a_2(t),a_3(t),a_4(t))$, showing a two-dimensional invariant torus in the KL decomposition of the $3H$ state.

The results from the KL decomposition are shown in Fig. 9(b) and the reconstruction with the six most energetic modes appears in Fig. 9(c). The time average (top snapshot) clearly captures the structure of the stationary outer ring and the rotations of the inner cells. It has an approximately $D_{11}\oplus O(2)$ spatial symmetry. The three most energetic pairs of KL modes (from top to bottom and left to right) $\Phi_1-\Phi_6$ are composed of the same Fourier–Bessel modes as in the $3H$ state, except that they appear in a different order. Using Eq. (2) we have verified that the modes in each pair have approximate D_3, D_2, and D_4 symmetry, respectively. As before, each pair forms an invariant subspace for the dynamics. On the $\{\Phi_1,\Phi_2\}$ subspace, the D_3 symmetry of the modes and the sinusoidal nature of the corresponding time coefficients provide a state with three traveling cells ($TW_3^{11/3H}$). Similarly, two traveling cells ($TW_2^{11/3H}$) are obtained on the $\{\Phi_3,\Phi_4\}$ subspace. Observe that both waves $TW_3^{11/3H}$ and $TW_2^{11/3H}$ are equivalent to those found in the $3H$ case, i.e., TW_3^{3H} and TW_2^{3H}, respectively. They all lie in equivalent subspaces. The frequency analysis further reveals that each wave undergoes uniform rotations. $TW_3^{11/3H}$ rotates with a slow angular speed of $\omega_3=6.14$ rad/s, while $TW_2^{11/3H}$ moves faster at $\omega_2=18.41$ rad/s. In this case, $\{\Phi_5,\Phi_6\}$ is a higher harmonic of $\{\Phi_3,\Phi_4\}$ and need not be included directly in the analysis.

The effects of changing the number of cells in the outer ring can be studied using results from the $12/3H$ hopping state. An analysis of its motion provides results very similar to those of the $11/3H$ state, with $\omega_2=19.88$ rad/s and $\omega_3=7.61$ rad/s.

In each of the above cases, two traveling waves are found to be lying in equivalent subspaces and with wave numbers two and three. Each wave rotates uniformly but the wave with two cells always moves faster. In the $11/3H$ and $12/3H$ states, the existence of a stationary outer ring has a negligible effect on the hopping motion of the inner ring.

C. Bifurcation analysis

Consider an idealization of the flame experiment by a Γ-equivariant system of ordinary differential equations (ODEs)

$$\dot{x}=f(x,\lambda), \tag{15}$$

where $\Gamma=O(2)$ models the symmetry of the burner, $x\in R^n$, and $\lambda\in R^2$ is a vector of parameters. We now wish to explain, within a mathematical context, how a pattern with three hopping cells can bifurcate from a system such as Eq. (15). As already discussed, the presence of a secondary ring of cells does not effect the hopping motion significantly. Consequently, our study is limited to the analysis of a single ring of hopping cells, which results from the interaction of two uniformly rotating waves with two and three cells, respectively. For generality these waves are labeled T_l and T_m, respectively. The subscripts specify the actual values of

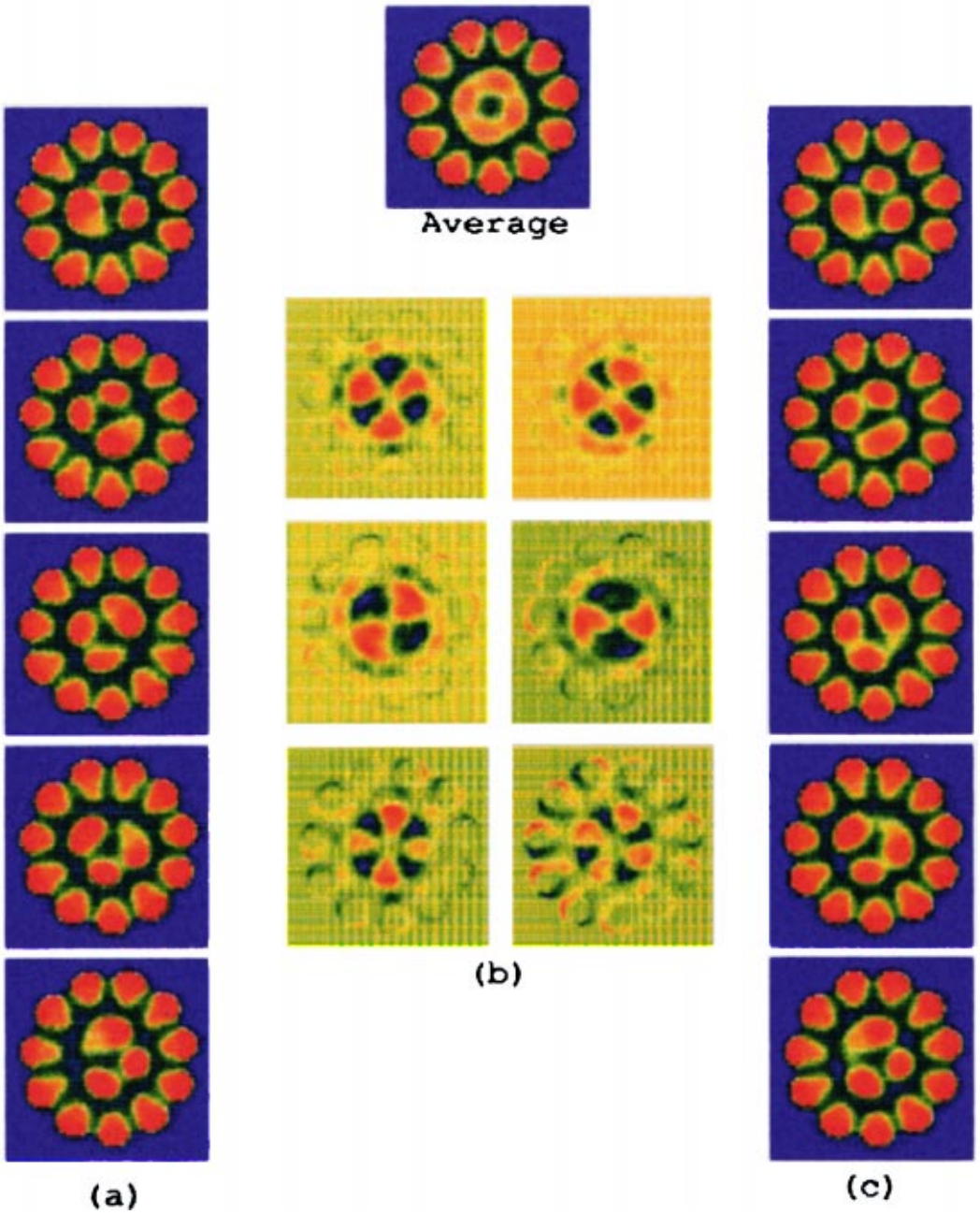

FIG. 9. KL decomposition of hopping motion in an inner ring with three cells surrounded by a stationary ring with eleven cells; (a) five instantaneous snapshots showing hopping motion in the inner ring as the cells rotate clockwise; (b) the time average of the data set appears at the top, followed (from left-to-right and top-to-bottom) by the six most energetic modes $\Phi_1-\Phi_6$; (c) the reconstruction of the dynamics using the six most energetic KL modes.

the wave numbers which are assumed to be relatively prime. In the present case, $l=2$ and $m=3$. Recall from Fig. 6(a) that each wave lies on an $O(2)$-invariant subspace created from the coupling of two KL modes

$$\begin{aligned} T_l:&\quad V_l=\text{span}\{\Phi_1,\Phi_2\},\\ T_m:&\quad V_m=\text{span}\{\Phi_3,\Phi_4\}. \end{aligned} \tag{16}$$

The KL modes and the periodicity of their time coefficients suggest that both traveling waves are created via Hopf bifurcations. We should then consider conditions, under the symmetries of the experiment, for these bifurcations to occur in Eq. (15). We assume that $x=0$ is the $O(2)$-symmetric ''trivial solution'' of the experiment satisfying

$$f(0,\lambda)=0, \tag{17}$$

and the linearization $L=(Df)_{0,0}$ has a pair of purely imaginary eigenvalues $\pm\omega_l i,\pm\omega_m i$, where ω_l and ω_m are incommensurate. Assume further that each pair of eigenvalues occurs twice so that $x\in R^8$. Since V_l and V_m are subspaces of dimension two, then a decomposition of R^8 takes the form

$$R^8=V_l\oplus V_l\oplus V_m\oplus V_m. \tag{18}$$

As indicated by the KL decomposition, the invariance of the subspaces implies that $L(V_l)\subset V_l$ and $L(V_m)\subset V_m$.

Under these assumptions, at $\lambda=0$, the $x=0$ uniform solution loses stability and two $O(2)$ symmetry-breaking branches of rotating waves are created simultaneously via a

Hopf bifurcation.[19] A competition between both waves corresponds to a Hopf–Hopf interaction between two $O(2)$ broken-symmetry modes. The dynamics of the mode interaction can be described through Eq. (15) in ''normal form,'' in which the terms in f are simplified (up to any order) through successive changes of coordinates. As in many other cases, the normal form can be deduced from the way the symmetry group Γ acts on the modes. Since two branches of Hopf bifurcations induce a torus action $T^2=S^1\times S^1$ on the system of ODEs, we must consider the action of $\Gamma\times T^2$ or $O(2)\times T^2$ on Eq. (15). Identifying R^8 with $C^2\oplus C^2$ as $(x_1,x_2,x_3,x_4,x_5,x_6,x_7,x_8)\mapsto(x_1+x_2i,x_3+x_4i,x_5+x_6i,x_7+x_8i)=(z_1,z_2,z_3,z_4)$, the action of $\Gamma\times T^2$ on $C^2\oplus C^2$ is generated by

$$\gamma(z_1,z_2,z_3,z_4)=(e^{l\gamma i}z_1,e^{-l\gamma i}z_2,e^{m\gamma i}z_3,e^{-m\gamma i}z_4) \quad \text{for all } \gamma\in SO(2), \tag{19}$$

$$\kappa(z_1,z_2,z_3,z_4)=(z_2,z_1,z_4,z_3) \quad \text{where } \kappa=\text{flip in } O(2), \tag{20}$$

$$(\theta_1,\theta_2)\cdot(z_1,z_2,z_3,z_4)=(e^{\theta_1 i}z_1,e^{\theta_1 i}z_2,e^{\theta_2 i}z_3,e^{\theta_2 i}z_4) \quad \text{for all } (\theta_1,\theta_2)\in T^2. \tag{21}$$

Observe that under this action $O(2)$ acts by l-fold rotations on V_l and m-fold rotations on V_m. For instance, consider V_l which according to Fig. 6(b), has roughly the form

$$R\{J_2e^{2xi},J_2e^{-2xi}\}. \tag{22}$$

In physical space, a spatial translation $x\mapsto x+\gamma$ in V_l corresponds to multiplication by $\{e^{2\gamma i},e^{-2\gamma i}\}$. The remaining group operations can be interpreted in a similar way. A normal form equation for an $O(2)\times T^2$ equivariant vector field f, under the action generated by Eqs. (19)–(21) takes the form

$$\begin{aligned}
\dot z_1&=(p_1(z)+iq_1(z))z_1\\
&\quad+(r_1(z)+is_1(z))\bar z_1^{m-1}z_2^m(z_3\bar z_4)^l,\\
\dot z_2&=(p_1(\kappa z)+iq_1(\kappa z))z_2\\
&\quad+(r_1(\kappa z)+is_1(\kappa z))z_1^m\bar z_2^{m-1}(\bar z_3z_4)^l,\\
\dot z_3&=(p_2(z)+iq_2(z))z_3\\
&\quad+(r_2(z)+is_2(z))(z_1\bar z_2)^m\bar z_3^{l-1}z_4^l,\\
\dot z_4&=(p_2(\kappa z)+iq_2(\kappa z))z_4\\
&\quad+(r_2(\kappa z)+is_2(\kappa z))(\bar z_1,z_2)^mz_3^l\bar z_4^{l-1},
\end{aligned} \tag{23}$$

where $z=(z_1,z_2,z_3,z_4)$, p_j, q_j, r_j, and $s_j(j=1,2)$ are functions of $|z_1|^2,\ldots,|z_4|^2$, $\mathrm{Re}\,\alpha$ and $\mathrm{Im}\,\alpha$, $\alpha=(z_1\bar z_2)^m(\bar z_3z_4)^l$, $p_1(0)=p_2(0)=0$, $q_1(0)=\omega_l$ and $q_2(0)=\omega_m$. Truncating at third order, we consider the following

$$\begin{aligned}
\dot z_1&=(\mu_1+a_{11}|z_1|^2+a_{12}|z_2|^2+a_{13}|z_3|^2+a_{14}|z_4|^2)z_1\\
&\quad+(\omega_l+b_{11}|z_1|^2+b_{12}|z_2|^2+b_{13}|z_3|^2+b_{14}|z_4|^2)iz_1,
\end{aligned}$$

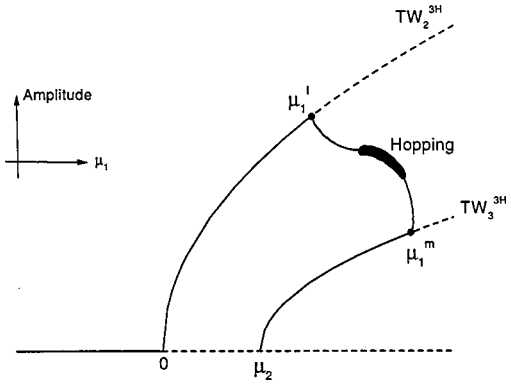

FIG. 10. Hopf–Hopf interaction of two branches of uniformly traveling cellular flames formed in an $O(2)$ symmetry breaking bifurcation from a uniform flame front. The mixed-mode solution is created through a secondary bifurcation. In physical space, the dynamics near the secondary bifurcation points appears as a standard MTW. In the middle, however, the behavior is radically different: three hopping cells similar to the experimental $3H$ state are observed.

$$\begin{aligned}
\dot z_2&=(\mu_1+a_{12}|z_1|^2+a_{11}|z_2|^2+a_{14}|z_3|^2+a_{13}|z_4|^2)z_2\\
&\quad+(\omega_l+b_{12}|z_1|^2+b_{11}|z_2|^2+b_{14}|z_3|^2+b_{13}|z_4|^2)iz_2,\\
\dot z_3&=((\mu_1-\mu_2)+a_{21}|z_1|^2+a_{22}|z_2|^2+a_{23}|z_3|^2\\
&\quad+a_{24}|z_4|^2)z_3+(\omega_m+b_{21}|z_1|^2+b_{22}|z_2|^2+b_{23}|z_2|^2\\
&\quad+b_{24}|z_4|^2)iz_3,\\
\dot z_4&=((\mu_1-\mu_2)+a_{22}|z_1|^2+a_{21}|z_2|^2+a_{24}|z_3|^2\\
&\quad+a_{23}|z_4|^2)z_4+(\omega_m+b_{22}|z_1|^2+b_{21}|z_2|^2+b_{24}|z_2|^2\\
&\quad+b_{23}|z_2|^2)iz_4,
\end{aligned} \tag{24}$$

where μ_1 and μ_2 are unfolding parameters. Periodic solutions, bifurcating from the trivial solution $z=0$, can be found by letting $z_j=r_je^{\theta_j i}$ and transforming the system (24) to polar coordinates. Up to conjugacy by the $Q(2)\times T^2$ action, we consider three types of periodic solutions—(a) l-mode solution: $r_2=r_3=r_4=0$, $r_1=(-\mu_1/a_{11})^{1/2}$; (b) m-mode solution: $r_1=r_2=r_3=0$, $r_4=(-\mu_2-\mu_1/a_{23})^{1/2}$; (c) mixed-mode solution: $a_{11}r_2^2+a_{13}r_4^2+\mu_1=0$, $a_{21}r_2^2+a_{23}r_4^2+\mu_1-\mu_2=0$.

Treating $\mu_2>0$ as a fixed auxiliary parameter, it can be verified that the trivial solution $z=0$ is stable for $\mu_1<0$ and unstable $\mu_1>0$. At $\mu_1=0$, a branch of l-mode solutions (T_l) bifurcates along the curve $r_1=(-\mu_1/a_{11})^{1/2}$. The bifurcation is supercritical when $\mu_1/a_{11}<0$, and subcritical otherwise. In physical space, the solution T_l is a cellular pattern with $l=2$ cells rotating uniformly at ω_l rad/s, and lies inside V_l which corresponds to the invariant subspace $z_2=z_3=z_4=0$. After μ_1 is further increased such that $\mu_1=\mu_2$, a branch of m-mode solutions (T_m) bifurcates along the curve $r_4=(\mu_2-\mu_1/a_{23})^{1/2}$. In this case, the bifurcation is supercritical when $(\mu_2-\mu_1)/a_{23}<0$, and subcritical otherwise. As before, T_m is a pattern with $m=3$ cells rotating uniformly at ω_m rad/s, and lies inside V_m which is the invariant subspace given by $z_1=z_2=z_3=0$. Note that a single point on both branches represents a circle of conjugate solutions.

Figure 10 shows a bifurcation diagram when $a_{11}=a_{12}$

$=-1$, $a_{13}=a_{14}=-1.5$, $a_{21}=a_{22}=-0.5$, $a_{23}=a_{24}=-1$, $b_{ij}=-1$, $\omega_2=1.178$ rad/frame (17.67 rad/s), and $\omega_3=0.859$ rad/frame (8.59 rad/s). These values were chosen to reflect the stability of the branches shown in the diagram. The mixed-mode branch is stable and lies in the invariant subspace $z_1=z_3=0$. A direct calculation shows that the mixed-mode solution bifurcates from the *l*-mode branch at $\mu_1^l=(a_{11}/a_{11}-a_{21})\mu_2$, and limits in the *m*-mode branch at $\mu_1^m=(a_{13}/a_{13}-a_{23})\mu_2$. A complete stability analysis is beyond the scope of this work and the interested reader is referred to Refs. 19 and 20.

Using DSTOOL,[21] we integrate Eq. (24) and traverse the bifurcation diagram along the mixed-mode branch. Since $z_1=z_3=0$, we only need to consider z_2 and z_4 and the four most energetic KL modes $\Phi_1-\Phi_4$ of Fig. 6(b). In physical space the evolution of the pattern takes the form

$$u(\mathbf{x},t)=\tilde{u}+\sum_{k=1}^{2}\mathrm{Re}\{z_{2k}(t)\}\Phi_{2k-1}(\mathbf{x}) + \mathrm{Im}\{z_{2k}(t)\}\Phi_{2k}(\mathbf{x}). \quad (25)$$

Near μ_1^l, the amplitude of z_2 is significantly larger than that of z_4, and the reconstruction produces a pattern of two cells rotating almost rigidly. Increasing μ_1 slightly does not seem to affect the rotational motion of the cells, but the shape modulations become more visible. The pattern continues to exhibit two cells. Similar behavior is observed near the other end of the branch, i.e., near μ_1^m. Since z_4 is now more dominant, the pattern contains three cells but the characteristics of the motion are similar. In both cases, the nature of the rotation coupled with shape variations produces a motion similar to (the MTW termed) ''ponies in a merry-go-around.''[4] However, away from the secondary bifurcations and near the middle of the branch, where z_2 and z_4 are comparable in magnitude, very different and interesting spatiotemporal behavior is produced. Figure 11 shows several snapshots of a movie generated by Eq. (25) near the middle of the mixed-mode branch. The emerging pattern contains three cells rotating counterclockwise but sequentially executing abrupt changes in their angular position. The direction of rotation can be easily controlled in Eq. (24), and the overall dynamics is consistent with the hopping motion of the experimental $3H$ state. In Fig. 12 various projections of the phase space (z_2,z_4) are shown. The motion is confined to a $2d$ torus similar to the one found in the experiment. Hopping motion in three cells results from the coupling of two Hopf-bifurcated states. Hopping motion in other configurations such as $11/3H$ and $12/3H$ can be reproduced in a similar way by substituting the appropriate average $\bar{u}$ in Eq. (25).

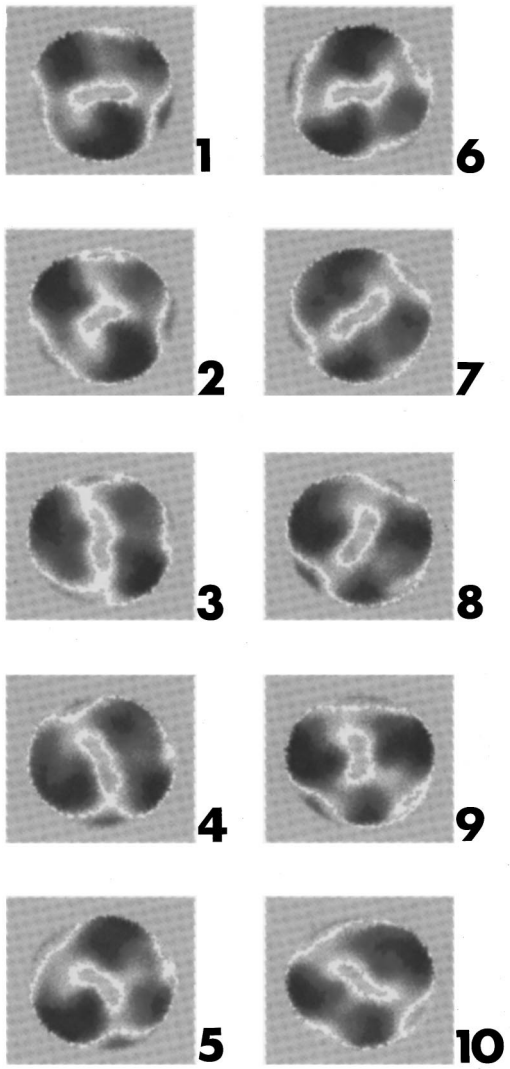

FIG. 11. Snapshots of the reconstructed dynamics of three hopping cells using normal form equations (24) and KL basis functions in physical space (25).

VI. GENERALIZATIONS TO OTHER HOPPING STATES

In this section, the results obtained for the $3H$, $11/3H$, and $12/3H$ states are compared with those for two other states: first, with a $10/2H$ state in which two cells hop inside a stationary ring with ten outer cells and, second, with a $4H$ state in which four cells hop in a single ring. This comparison will identify the common characteristics among hopping states with different numbers of cells.

Figure 13(a) shows five sequential snapshots of the $10/2H$ state. A stationary outer ring with ten cells surrounds an inner ring with two cells hopping counterclockwise. The motion in the inner ring is similar to the hopping motion with three cells. At a given instant, one of the two cells is moving rapidly, or hopping, while the other is almost stationary. In addition, the hopping cell is more asymmetric than the other cell. This dynamics is very different from the modulated rotating cells obtained from the interaction of two steady modes in a 1:2 ratio[15,22] in which the shapes of both cells (which changed periodically) were identical at all times.

Figure 13(b) shows the results from the KL decomposition of the $10/2H$ state. The time average (top snapshot) captures the structure of the ten cells in the stationary outer ring and the rotation of the two inner cells. The average pattern has an approximately $D_{10}\oplus O(2)$ spatial symmetry. The energy spectra $E=(23.02, 18.72, 9.94, 9.69, 4.84, 4.81,...)$, indicates an equal distribution of energy among pairs of KL modes (shown from top to bottom and left to right) $\Phi_1-\Phi_6$. Using Eq. (2), we find that each pair has D_2,

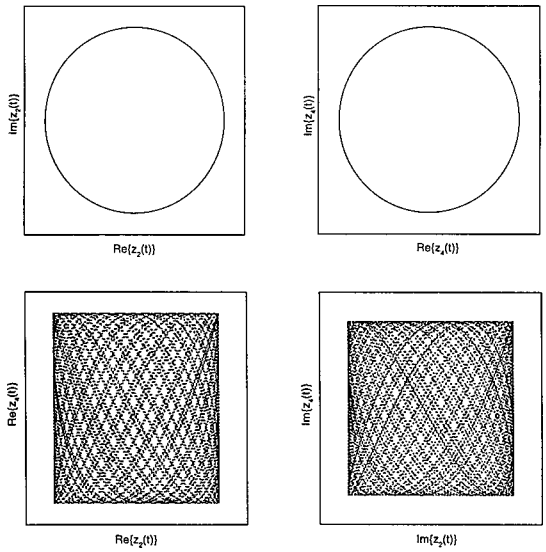

FIG. 12. Projections of phase plane $(z_2(t), z_4(t))$ showing a two-dimensional invariant torus in the normal form reconstruction of the $3H$ state. Observe the similarities with the torus shown in Fig. 8.

D_1, and D_3 symmetry, respectively. In physical space, $\{\Phi_1, \Phi_2\}$ forms a uniformly traveling wave with two cells rotating slowly at an angular speed $\omega_2 = 15.645$ rad/s, approximately. Similarly, $\{\Phi_3, \Phi_4\}$ creates a uniformly traveling wave with one cell rotating rapidly at an angular speed

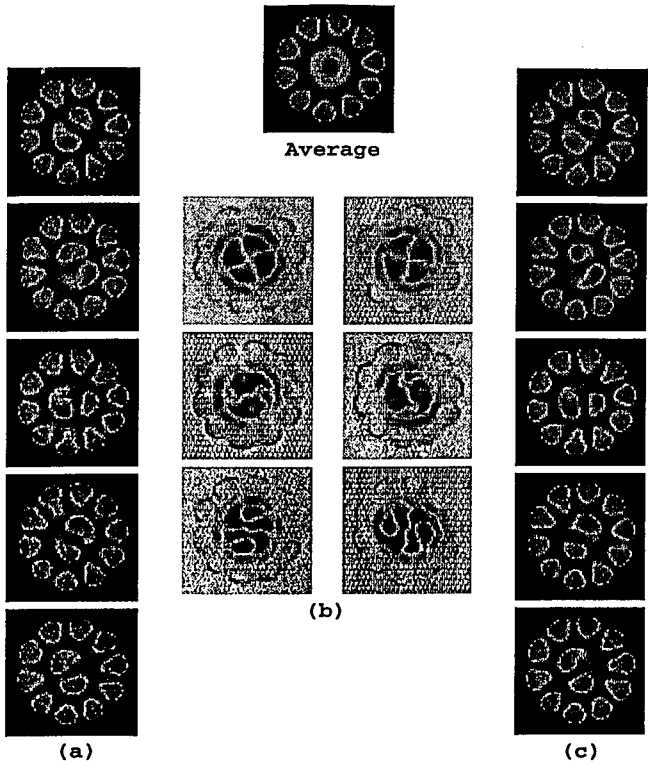

FIG. 13. KL decomposition of hopping motion in an inner ring with two cells surrounded by a stationary ring with ten cells; (a) five instantaneous snapshots showing hopping motion in the inner ring as the two cells rotate counterclockwise; (b) the time average of the data set appears at the top, followed (from left-to-right and top-to-bottom) by the six most energetic modes $\Phi_1 - \Phi_6$; (c) the reconstruction of the dynamics using the six most energetic KL modes.

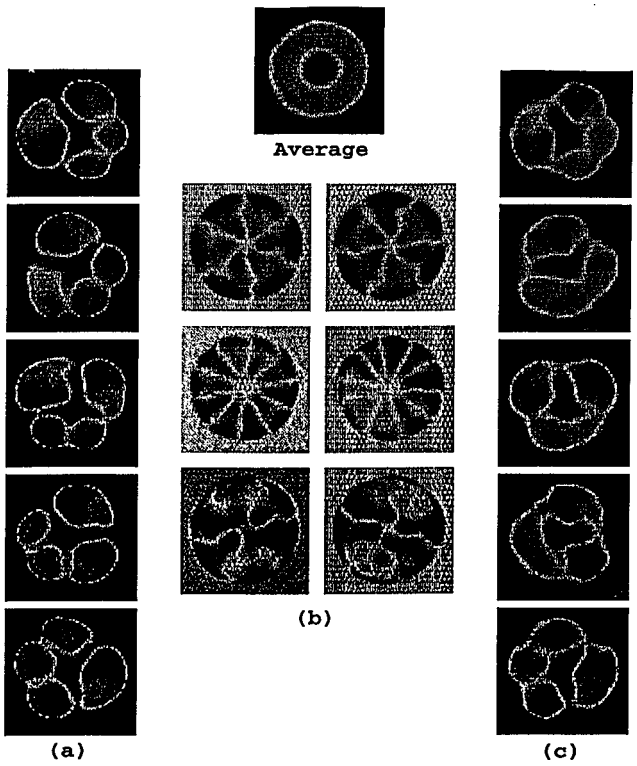

FIG. 14. KL decomposition of hopping motion in a single ring state with four cells (a) five instantaneous snapshots showing hopping motion as the cells rotate counterclockwise; (b) the time average of the data set appears at the top, followed (from left-to-right and top-to-bottom) by the six most energetic modes $\Phi_1 - \Phi_6$; (c) the reconstruction of the dynamics using the six most energetic KL modes.

$\omega_1 = 46.755$ rad/s, approximately. The reconstruction with the six most energetic modes is shown in Fig. 13(c).

The hopping state labeled $4H$ is shown in Fig. 14(a). Five sequential snapshots depict a single ring pattern of four cells hopping counterclockwise. As in previous cases, the instantaneous asymmetry of a single cell is clearly visible. The modes extracted from the KL decomposition are shown in Fig. 14(b). The time average (top snapshot) now captures the $O(2)$ symmetry of the burner. The energy spectra $E = (13.5, 13.5, 13.3, 13.3, 7.0, 7.0, ...)$, indicates an equal distribution of energy among pairs of KL modes $\Phi_1 - \Phi_6$. Using Eq. (2), we find that each pair has D_3, D_5, and D_4 symmetry, respectively. In physical space, $\{\Phi_1, \Phi_2\}$ forms a TW with three cells rotating at an angular speed $\omega_3 = 9.8$ rad/s, while $\{\Phi_3, \Phi_4\}$ creates a TW with four cells rotating at an angular speed of $\omega_4 = 4.23$ rad/s. The reconstruction with the six most energetic modes is shown in Fig. 14(c) for illustration purposes.

The analysis and conclusions about hopping motion in n cells were obtained based on the assumption that only one cell hops at a time, while the other cells are almost stationary. This result is consistent with almost all of the experimental observations. The mathematical description presented throughout this work predicts the existence of other forms of hopping motion. For instance, a state where more than one cell hops simultaneously is possible. This dynamics bifurcates from similar branches of TWs except that now the wave numbers would be n and $n-2$. An example of a double

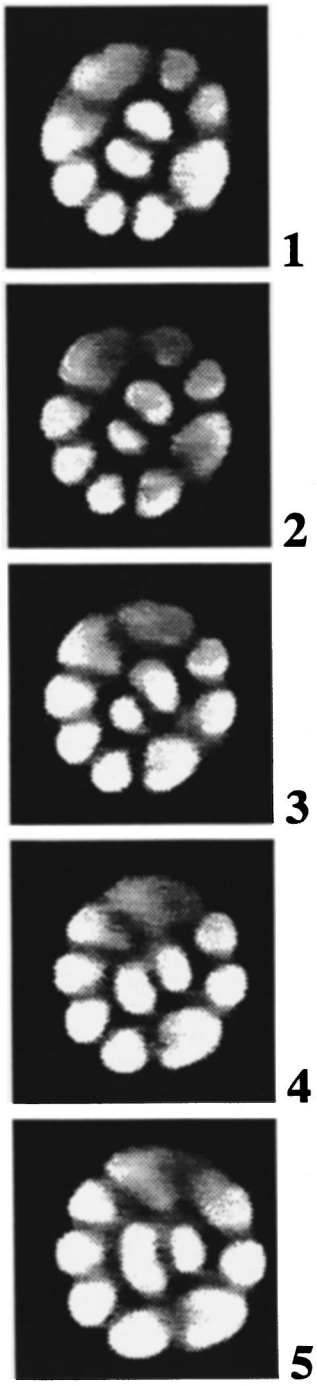

FIG. 15. Five sequential frames of videotape depicting the motion of a double-hopping state.

hopping state with $n=8$ cells was indeed found in reviewing old data from the experiment. In Fig. 15 five consecutive frames of videotape are presented from a state in which two pairs of cells on opposite sides of the outer ring are simultaneously executing hopping motion.

VII. CONCLUSION

In this work we have extended the modal analysis used to describe the characteristics of low dimensional dynamics in concentric rings of cellular flames to the study of hopping states, and we have shown how hopping motion is significantly different from the motions of the other states. The overall results can be generalized to a ring with n cells. Hopping states bifurcate from a Hopf–Hopf symmetry breaking interaction of two uniformly traveling waves $(\mathrm{TW}_n, \mathrm{TW}_{n-1})$ with wave numbers n and $n-1$. TW_{n-1} rotates faster than TW_n. In physical space, the dynamics can be reconstructed through the normal form equations (23) with $l=n-1$ and $m=n$.

A hopping state is formed by the interaction of two traveling waves of asymmetric cells moving at different speeds; yet, it is not a traveling wave and some of its cells are symmetric. For $N>2$ at least one cell is at rest and symmetric at any time. Therefore, unlike TWs or MTWs, one cannot go into a rotating frame at the speed of (either) traveling wave and eliminate one of the frequencies. At either end of the branch, near the secondary bifurcation, one of the the traveling waves dominates; but, as the amplitudes of the two modes become comparable, the traveling wave character of the resultant state disappears and hopping motion is observed.

This result is one of the most interesting issues regarding the geometry of the underlying phase space. Because the number of cells is not the same near the bifurcating points, it is an open question as to how the two $2d$ tori are connected. We intend to study this problem both numerically in the model and experimentally by taking data along the mixed mode branch.

ACKNOWLEDGMENTS

The authors would like to thank M. Golubitsky, B. Matkowsky, I. Melbourne, and K. Robbins for many useful discussions and suggestions. This work has been partially funded by the Office of Naval Research through Grant No. N-00014-K-0613, and from the Energy Laboratory at The University of Houston.

APPENDIX: PROPERTIES OF KARHUNEN–LOÈVE DECOMPOSITION

The two-point correlation matrix of Eq. (9) is Hermitian. That is, $r(\mathbf{x},\mathbf{y})=r^*(\mathbf{y},\mathbf{x})$. The matrix then admits according to Riesz's theorem,[23] a diagonal decomposition of the form

$$r(\mathbf{x},\mathbf{y})=\sum_{k=1}^{N}\lambda_k\Phi_k(\mathbf{x})\Phi_k^*(\mathbf{y}). \tag{A1}$$

This fact is particularly useful when finding the KL modes analytically. They can be read off from the diagonal decomposition (26). The following proposition states that the KL basis functions and time coefficients are uncorrelated in space and time, respectively.[24–29]

Proposition 1: The KL modes $\{\Phi_k(\mathbf{x})\}$, with corresponding temporal coefficients $\{a_k(t)\}$, satisfy the following orthogonality properties: (i) $\Phi_j^*(\mathbf{x})\Phi_k(\mathbf{x})=\delta_{jk}$, (ii) $\langle a_j(t)a_k^*(t)\rangle=\delta_{jk}\lambda_j$, where δ_{jk} represents the Kronecker delta function.

Property (ii) is obtained when the terms in the diagonal decomposition (A1) are compared with the expression $r(\mathbf{x},\mathbf{y})=\Sigma\langle a_j(t)a_k^*(t)\rangle\Phi_j(\mathbf{x})\Phi_k^*(\mathbf{y})$. The non-negative and self-adjoint properties of $r(\mathbf{x},\mathbf{y})$ imply that all eigenvalues

are non-negative and can be ordered accordingly: $\lambda_1 \geqslant \lambda_2 \cdots \geqslant \cdots \geqslant 0$. Statistically speaking, λ_k represents the variance of the data set in the direction of the corresponding KL mode $\Phi_k(\mathbf{x})$. In physical space, if u represents a component of a velocity field, then λ_k measures the amount of ''kinetic energy'' captured by the respective KL mode $\Phi_k(\mathbf{x})$. In this sense, the energy measures the contribution of each mode to the overall dynamics. The total energy captured in a Karhunen–Loève decomposition is then defined as the sum of all eigenvalues

$$E = \sum_{k=1}^{N} \lambda_k . \tag{A2}$$

Each KL mode $\Phi_k(\mathbf{x})$ captures a portion of the total energy and is defined as the *relative energy*

$$E_k = \frac{\lambda_k}{\Sigma_{j=1}^{N} \lambda_j}. \tag{A3}$$

The relative energy measures the contribution of each eigenvector $\Phi_k(\mathbf{x})$ to the overall dynamics in the reconstruction given by Eq. (7).

Equation (8) states that Karhunen–Loève decomposition produces a basis that minimizes the least-squares truncation error. This property can also be stated in terms of the energy captured by the KL modes.

Proposition 2: Let $\{a_k(t), \Phi_k(\mathbf{x})\}$ be the KL-basis pairs obtained from a scalar field $u(\mathbf{x},t)$, satisfying Eqs. (7), (A1), and (13). Let $\{b_k(t), \Psi_k(\mathbf{x})\}$ be any arbitrary orthonormal basis pair satisfying Eq. (7). The KL basis is optimal in the sense that the total cumulative energy captured by the sequence $\{a_k(t), \Phi_k(\mathbf{x})\}$ is always greater or equal to the total cumulative energy captured by $\{b_k(t), \Psi_k(\mathbf{x})\}$, provided that the number of eigenfunctions (respecting their ordering from most to least energetic) employed is the same. Formally

$$\sum_{k=1}^{N} E_k = \sum_{k=1}^{N} \langle a_k(t) a_k^*(t) \rangle = \sum_{k=1}^{N} \lambda_k \geqslant \sum_{k=1}^{N} \langle b_k(t) b_k^*(t) \rangle . \tag{A4}$$

[1] A. Palacios, G. Gunaratne, and M. Gorman, ''Cellular pattern formation in circular domains,'' Chaos **7**, 463 (1997).

[2] M. Gorman, M. el-Hamdi, and K. Robbins, ''A Picturebook of Dynamical Modes of Flat, Laminar Premixed Flames,'' Technical Report No. 2, University of Houston, 1990.

[3] M. Gorman, M. el-Hamdi, and K. Robbins, ''Hopping motion in ordered states of cellular flames,'' Combust. Sci. Technol. **98**, 71 (1994).

[4] A. Bayliss, B. Matkowsky, and H. Riecke, ''Structure and dynamics of modulated traveling waves in cellular flames,'' Physica D **74**, 1 (1994).

[5] G. H. Gunaratne, M. el-Hamdi, M. Gorman, and K. Robbins, ''Asymmetric cells and rotating rings in cellular flames,'' Mod. Phys. Lett. B **10**, 1379 (1996).

[6] A. Bayliss, and B. Matkowsky, ''Nonlinear dynamics of cellular flames,'' SIAM (Soc. Ind. Appl. Math.) J. Appl. Math. **52**, 396 (1992).

[7] L. Sinay and F. Williams, ''An analytical approach to the description of nonadibatic cellular flames near extinction,'' SIAM (Soc. Ind. Appl. Math.) J. Appl. Math. **52**, 416 (1992).

[8] G. Sivashinsky, ''Nonlinear analysis of hydrodynamic instability in laminar flames. I. Derivation of basic equations,'' Acta Astraunica **4**, 1177 (1977).

[9] W. Press, S. Teukolsky, W. Vetterling, and B. Flannery, *Numerical Recipes in C* (Cambridge University Press, New York, 1994).

[10] G. Watson, *A Treatise on the Theory of Bessel Functions* (Cambridge University Press, Cambridge, 1962).

[11] P. Holmes, J. Lumley, and G. Berkooz, *Turbulence, Coherent Structures, Dynamical Systems and Symmetry* (Cambridge University Press, Cambridge, 1996).

[12] K. Karhunen, ''Zur spektraltheorie stochasticher prozesse,'' Ann. Acad. Sci. Fenn., Ser. AI: Math. **I**, 34 (1944).

[13] M. Loève, *Probability Theory* (Van Nostrand, New York, 1995).

[14] J. L. Lumley, ''The structure of inhomogeneous turbulent floes,'' in *Atmospheric Turbulence and Radio Wave Propagation*, edited by A. M. Yaglom and V. I. Tatarski (Nauka, Moscow, 1967), p. 166.

[15] L. Sirovich, ''Turbulence and the dynamics of coherent structures. I. Coherent structures,'' Q. Appl. Math. **5**, 561 (1981).

[16] D. Walgraef, *Spatio-temporal Pattern Formation* (Springer, New York, 1977).

[17] D. Armbruster, R. Heiland, and E. Kostelich, ''KLTOOL: A tool to analyze spatiotemporal complexity,'' Chaos **4**, 421 (1993).

[18] M. Dellnitz, M. Golubitsky, and M. Nicol, ''Symmetry of attractors and the Karhunen–Loève decomposition'' in *Trends and Perspectives in Applied Mathematics*, edited by L. Sirovich, Vol. 100, p. 73.

[19] M. Golubitsky, I. Stewart, and D. G. Schaeffer, *Singularities and Groups in Bifurcation Theory* (Springer, New York, 1988), Vol. 2.

[20] P. Chossat, M. Golubitsky, and B. Keyfitz, ''Hopf–Hopf mode interactions with $O(2)$ symmetry,'' Dyn. Stab. Sys. **1**, 255 (1987).

[21] J. Guckenheimer, M. Myers, F. Wicklin, and P. Worfolk, ''DSTOOL: A Dynamical System Toolkit with an Interactive Graphical Interface,'' Technical Report, Cornell University, 1995.

[22] D. Armbruster, J. Guckenheimer, and P. Holmes, ''Heteroclinic cycles and modulated traveling waves in system with $O(2)$ symmetry,'' Physica D **29**, 257 (1988).

[23] F. Riesz and B. Sz.-Nagy, *Functional Analysis* (Dover, New York, 1990).

[24] *The Mathematics of Combustion*, edited by J. Buckmaster (SIAM, Philadelphia, 1985).

[25] M. Gorman, C. Hamill, M. el-Hamdi, and K. Robbins, ''Rotating and modulated rotating states of cellular flames,'' Combust. Sci. Technol. **98**, 25 (1994).

[26] M. Gorman, M. el-Hamdi, and K. Robbins, ''Experimental observation of ordered states of cellular flames,'' Combust. Sci. Technol. **98**, 37 (1994).

[27] M. Gorman, C. Hamill, M. el-Hamdi and K. Robbins, ''Four types of chaotic dynamics in cellular flames,'' Combust. Sci. Technol. **98**, 79 (1994).

[28] Y. Kuramoto, ''Diffusion induced chaos in reaction systems,'' Suppl. Prog. Theor. Phys. **64**, 346 (1978).

[29] A. Turing, ''The chemical basis of morphogenesis,'' Philos. Trans. R. Soc. London, Ser. B **237**, 37 (1952).